

Axion and dark photon limits from Crab Nebula high energy gamma-rays

Xiaojun Bi^{1,2}, Yu Gao^{1,*}, Jinguang Guo^{1,2,†}, Nick Houston³, Tianjun Li^{4,2}, Fangzhou Xu^{5,4}, and Xin Zhang^{6,7}

¹ Key Laboratory of Particle Astrophysics, Institute of High Energy Physics,
Chinese Academy of Sciences, Beijing, 100049, China

² School of Physical Sciences, University of Chinese Academy of Sciences, Beijing, 100049, China

³ Institute of Theoretical Physics, Faculty of Science,
Beijing University of Technology, Beijing 100124, China

⁴ Key Laboratory of Theoretical Physics, Institute of Theoretical Physics,
Chinese Academy of Sciences, Beijing 100190, China

⁵ Institute of Modern Physics, Tsinghua University, Beijing 100084, China

⁶ Key Laboratory of Computational Astrophysics, National Astronomical Observatories,
Chinese Academy of Sciences, Beijing, 100012, China and

⁷ School of Astronomy and Space Science, University of Chinese Academy of Sciences, Beijing 100049, China

The observation of cosmic sub-PeV gamma-rays from the Crab Nebula opens up the possibility of testing cosmic ray photon transparency at the multi-hundred TeV scale. Assuming no deviation from a source gamma-ray emission due to accelerated electron inverse-Compton scattering, higher event energies can extend constraints on the effects of new physics; we consider oscillation between gamma-rays and axions, plus attenuation effects from gamma-ray absorption in the case of dark photon dark matter. Combining the recent AS γ and HAWC sub-PeV data with earlier MAGIC and HEGRA data, axion-like particles are most constrained in the $2 \times 10^{-7} - 6 \times 10^{-7}$ eV mass range, where the coupling $g_{a\gamma\gamma}$ is constrained to be below 1.8×10^{-10} GeV⁻¹. Direct scattering from dark photon dark matter limits kinetic mixing $\epsilon \lesssim 10^{-3}$ for masses between 0.01 and 1 eV.

I. INTRODUCTION

Very high energy cosmic photons are crucial astrophysical observational targets, as they can help us to both understand acceleration mechanisms at high energies and identify cosmic ray sources via their directional information. However, very high energy gamma rays above 100 TeV are rare occurrences due to both the scarcity of nearby sources, and the attenuation effect of scattering from the cosmic microwave background (CMB) and extragalactic background light (EBL), reducing their visibility from distant extra-galactic sources [1]. Recently, the highest sub-PeV gamma rays from the Crab Nebula events were detected by the Tibet AS γ experiment [2]. The Crab Nebula is a well-known high energy gamma ray source, arising possibly due to acceleration processes in the magnetized wind created by the central pulsar. High energy gamma rays in the TeV range originating therefrom have been measured by a number of experiments, including HEGRA [3], MAGIC [4], HESS [5], etc. The latest data from Tibet AS γ [2] and HAWC [6] increase the observed gamma ray spectrum to energies above 100 TeV.

Besides astrophysical interests, the propagation of extremely high energy gamma rays can test photon interactions from theories beyond the Standard Model (BSM). Well-motivated scenarios include photon mixing into low-mass bosonic states like axions [7] and dark photons [8, 9], photon decay via Lorentz invariance violation [10, 11], etc. The Crab Nebula is a major Galactic source of

high energy gamma rays, and the high energy scale of its gamma ray spectrum is utilized for constraining Lorentz invariance violation [12].

BSM processes often lead to an energy-dependent photon flux reduction that benefits from higher energy scales of observed gamma rays. In this paper we study the attenuation of gamma ray survival probability from two new-physics processes induced by an axion-like pseudoscalar or a dark photon. In comparison with previous cosmic ray measurements, we demonstrate that the newly observed high energy gamma ray data enhances the constraints on photon interactions with these new light bosons.

Originally proposed as a natural solution to the strong CP problem [13–15], the QCD axion has recently enjoyed increased attention as a non-thermal dark matter candidate [16, 17] within a well-motivated yet evasive parameter space: fulfilling the correct relic density requires the axion mass to be around 10^{-5} eV and the decay constant $f \sim 10^{12}$ GeV. In addition, generalized axion-like particles (ALPs) are light pseudoscalars that carry a similar $\frac{a}{f} F\tilde{F}$ coupling to photons. ALPs are commonly predicted in grand unified and superstring theories but they are not restricted to a particular mass range. The mass of the QCD axion is directly related to the scale of its couplings, however for ALPs there is in general no such constraint [18]. Axions and ALPs are being searched for by a number of experiments (see [19] for a recent review). For high energy cosmic gamma rays, axions and ALPs can cause oscillation effects through their coupling to two photons in the presence of galactic magnetic fields [20], as explored in recent studies on potential spectral distortions from astrophysical gamma ray sources [21–51].

Dark photons [52, 53] are the gauge bosons of hidden

* gaoyu@ihep.ac.cn

† guojg@ihep.ac.cn

sector $U(1)$ gauge symmetries under which the Standard Model (SM) particles are not directly charged. The dark photons may kinetically mix with the SM photon, allowing normal matter to acquire a small coupling to the mixed state. Such a mixing causes photon-dark photon oscillation in the case where the dark photon has nonzero mass, which also enables cosmic photons to scatter off environmental dark photons [54], if in particular the dark photon makes up the dark matter in our Universe. Both effects attenuate energetic gamma rays over long propagation distances, as explored in a number of studies [55–58].

In the following Sections II - III we briefly discuss ALP-photon oscillation and scattering effects by dark photon on gamma rays, respectively. In Section IV we analyze the compilation of Tibet AS γ , HEGRA, MAGIC and HAWC data, and give new physics limits by testing the attenuation processes, and then finally conclude in Section V.

II. PHOTON-ALP OSCILLATION

An ALP a couples to photons with the characteristic coupling

$$\mathcal{L}_{a\gamma\gamma} = -\frac{1}{4f} a F \tilde{F} = \frac{a}{f} \vec{E} \cdot \vec{B}, \quad (1)$$

where f relates to the axion decay constant f_a by $f^{-1} = c_\gamma \alpha / (\pi f_a)$, α is the fine structure constant and c_γ is a model dependent coefficient dependent on the underlying theory, e.g. $c_\gamma = -0.97$ and 0.36 in KSVZ [59, 60] and DFSZ [61, 62] models, respectively. For ALPs, here we focus on $g_{a\gamma\gamma} \equiv f^{-1}$ as the sole effective parameter for phenomenological purposes. In the presence of an external magnetic field B , Eq. (1) becomes a mixing term [7] between the ALP and a photon that allows for oscillation between the ALP and photon polarisations. The propagating mode is described by the three component vector $\Psi = (A_1, A_2, a)^T$, where $A_{1,2}$ are the photon polarisations in the transverse $\{\hat{x}, \hat{y}\}$ plane, and the propagation direction is \hat{z} . The propagation of Ψ is then governed by the equation [63]

$$(\omega - i \frac{d}{d\ell} + \mathcal{M}) \Psi = 0, \quad (2)$$

where ℓ donates the propagation distance and \mathcal{M} accounts for mixing-induced oscillation and scattering processes. Choosing the transverse projection of the external magnetic field B_T to be along the \hat{y} direction, \mathcal{M} can be written as

$$\mathcal{M} = \begin{pmatrix} \Delta_\perp & & \\ & \Delta_\parallel & \Delta_{a\gamma} \\ & \Delta_{a\gamma} & \Delta_{aa} \end{pmatrix} + i \begin{pmatrix} \Gamma_{BG} & & \\ & \Gamma_{BG} & \\ & & 0 \end{pmatrix}. \quad (3)$$

The first term gives photon-ALP mixing, in which

$$\begin{aligned} \Delta_\perp &= \Delta_{\text{pl}} + 2\Delta_{\text{QED}} + \Delta_{\text{dis}}, \\ \Delta_\parallel &= \Delta_{\text{pl}} + \frac{7}{2}\Delta_{\text{QED}} + \Delta_{\text{dis}}, \end{aligned} \quad (4)$$

and the Faraday effect is neglected. Δ_{pl} corresponds to an effective photon mass $-\omega_{\text{pl}}^2/(2E)$ due to the presence of free charges, where E is the photon energy and $\omega_{\text{pl}} = \sqrt{4\pi\alpha n_e/m_e}$ is the plasma frequency with the electron density n_e and electron mass m_e . $\Delta_{\text{QED}} = \alpha E/(45\pi)(B/B_{\text{cr}})^2$ accounts for the QED vacuum polarisation effect, where the critical magnetic field B_{cr} equals $m_e^2/|e| \sim 4.4 \times 10^{13}$ G [64]. $\Delta_{\text{dis}} = 44\alpha^2 E \rho_{\text{RF}}/(135m_e^4)$ accounts for dispersion effects from photon-photon scattering on environmental radiation field [65], where the energy density ρ_{RF} includes both the CMB and the interstellar radiation field (ISRF) contributions. The QED vacuum polarisation and dispersion effects evaluate to a small $\mathcal{O}(10^{-5})$ correction to the survival probability of 100 TeV photons from the Crab Nebula. These effects are practically negligible and we do not consider these effects in the following analysis. ALP parameters include the mixing term $\Delta_{a\gamma} = g_{a\gamma\gamma} B_T/2$ and the diagonal term $\Delta_{aa} = -m_a^2/(2E)$, where m_a is the ALP mass.

The second term $i\Gamma_{\text{BG}}$ accounts for the absorption of high energy photons via the $\gamma\gamma \rightarrow e^+e^-$ process, where the absorption rate $\Gamma_{\text{BG}} = 1/(2\lambda)$ and λ is the photon mean free path in the presence of background photons. The energy threshold for e^+e^- production is

$$E_{\text{th}} \sim \frac{2m_e^2}{E_{\text{BG}}} \sim 0.5 \left(\frac{1\text{eV}}{E_{\text{BG}}} \right) \text{TeV}, \quad (5)$$

where E_{BG} is the photon energy in the background radiation field, i.e. the CMB and the ISRF. For photons from the Crab Nebula, the ISRF intensity causes a stronger absorption effect and we use the ISRF model in Ref. [66]. The absorption rate is obtained by the $\gamma\gamma$ scattering cross-section weighted by the background radiation field energy spectrum n_{BG} ,

$$\lambda^{-1} = \int dE_{\text{BG}} \frac{dn_{\text{BG}}}{dE_{\text{BG}}} \hat{\sigma}, \quad (6)$$

$$\hat{\sigma} = \int_0^2 dx \frac{x}{2} \sigma_{\gamma\gamma}, \quad (7)$$

where $x = 1 - \cos\theta_{\gamma\gamma}$, $\theta_{\gamma\gamma}$ is the angle between incident photons, and the hard scattering $\sigma_{\gamma\gamma}$ is given by

$$\begin{aligned} \sigma_{\gamma\gamma} &= \frac{3}{16} \sigma_{\text{T}} (1 - \beta^2) \\ &\times \left[(3 - \beta^4) \ln \frac{1 + \beta}{1 - \beta} - 2\beta(2 - \beta^2) \right], \end{aligned} \quad (8)$$

$$\beta \equiv (1 - 4m_e^2/s)^{1/2}, \quad (9)$$

where σ_{T} is the Thomson cross section and $s = 2xE E_{\text{BG}}$ is the Mandelstam variable. For 100 TeV photons from the Crab Nebula, this absorption would result in a loss

of $\sim 10^{-2}$ of the photon flux, with smaller losses at lower energies.

In case B_T is not strictly along \hat{y} but at an angle ψ to \hat{y} , the \mathcal{M} matrix is modified by a rotation,

$$\mathcal{M} = V(\psi)\mathcal{M}_0V^\dagger(\psi), \quad (10)$$

$$V(\psi) = \begin{pmatrix} \cos\psi & \sin\psi & 0 \\ -\sin\psi & \cos\psi & 0 \\ 0 & 0 & 1 \end{pmatrix}. \quad (11)$$

The Galactic magnetic field consists of a random component with small coherence scales and a large-scale regular component. The random component leads to self-cancellation in oscillation and is ignored in our analysis. We consider the regular Galactic B -field model in Ref. [67], and propagate unpolarised photons through a binned distribution of B_T between the Crab Nebula and the Earth, where its average magnitude is around 1.3 μG . For the binned/sliced B_T distribution, the magnitude and direction of B_T vary between distance-slices, yet within each slice the B_T is considered uniform. The photon survival probability is derived by numerically solving the density matrix evolution equation [23, 28, 51]

$$i\frac{d\rho}{d\ell} = [\rho, \mathcal{M}], \quad (12)$$

where $\rho = \Psi\Psi^\dagger$. For initially unpolarised photons, $\rho(0)$ takes the initial values $1/2 \text{diag}(1, 1, 0)$. The final density matrix $\rho(L)$ is the density matrix at Earth where L represents the total distance between Crab Nebula and Earth. After considering the photon-ALP oscillation effect and the absorption effect, the survival probability of a photon $P_{\text{sur.}} = \rho_{11}(L) + \rho_{22}(L)$ where ρ_{11}, ρ_{22} represent the first and second diagonal elements in the density matrix. The observed gamma ray flux is then

$$\frac{d\phi}{dE} = P_{\text{sur.}} \cdot \left. \frac{d\phi}{dE} \right|_{\text{source}}. \quad (13)$$

III. PHOTON-DARK PHOTON SCATTERING

In extensions of the SM featuring dark photons γ' with vector $U(1)$ potential A_D^μ , their interactions are introduced via terms of the type

$$\mathcal{L}_{\text{SM}\otimes\text{D}} = -\epsilon e J_\mu^{\text{SM}} A_D^\mu, \quad (14)$$

where ϵ is a dimensionless mixing parameter and J_μ^{SM} is the SM electromagnetic current [68]. At energies above that of the dark photon mass but below that of the corresponding fermion mass, these operators can be integrated out to yield the familiar low-energy interactions

$$\mathcal{L} \supset -\frac{1}{4}\mathcal{F}^{\mu\nu}\mathcal{F}_{\mu\nu} - \frac{\epsilon}{2}\mathcal{F}^{\mu\nu}\mathcal{F}'_{\mu\nu} - \frac{1}{4}\mathcal{F}'^{\mu\nu}\mathcal{F}'_{\mu\nu}. \quad (15)$$

We use A (A_D) to represent photon (the dark photon) state, respectively. Due to the mixing between dark photon and ordinary photon, we will consider the $A - A_D$

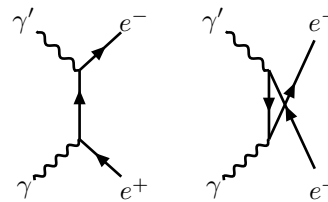


FIG. 1. Photon attenuation diagrams for $\gamma - \gamma'$ scattering.

scattering case when the dark photon constitutes the dark matter in our Galaxy. If the dark photon is massive the scattering process $\gamma\gamma' \rightarrow e^+e^-$ kinematically opens up for gamma rays above the energy threshold

$$E > E'_{\text{th}} = \frac{2m_e^2}{m_D}, \quad (16)$$

and 10^2 TeV gamma rays reach this threshold for m_D down to 10^{-2} eV scale. At the leading order the cosmic ray photon can scatter from the two transversely polarized dark photon modes due to a coupling to the electron via mixing with the QED photon. The corresponding Feynman diagrams are shown in Fig. 1. The resulting scattering cross-section is

$$\sigma_D = \frac{8\pi\epsilon^2\alpha^2}{3(s - m_D^2)^3} \left[-\beta(s^2 + 4sm_e^2 + m_D^4) + \ln\left(\frac{1+\beta}{1-\beta}\right) (s^2 + 4sm_e^2 + m_D^4 - 4m_D^2m_e^2 - 8m_e^4) \right], \quad (17)$$

where $\beta = \sqrt{1 - 4m_e^2/s}$ and $s = 2Em_D + m_D^2$ is the usual Mandelstam variable. Eq. (17) reduces to photon-photon scattering cross-section up to a factor $2\epsilon^2/3$ when $m_D = 0$ due to the absence of the longitudinal mode of the photon.

If the dark photon makes up the major component of the cold dark matter in our Universe, the corresponding mean free path of photon propagation is

$$\lambda = \frac{1}{n_D\sigma_D} + (2\Gamma_{\text{BG}})^{-1}, \quad (18)$$

where the dark photon density $n_D = \rho_{\text{DM}}/m_D$ follows from that of the Galactic dark matter distribution, $\rho_{\text{DM}} = 0.3 \text{ GeV cm}^{-3}$. The second term accounts for absorption due to the background radiation. The observed gamma ray flux is then

$$\frac{d\phi}{dE} = (1 - P_{\text{abs.}}) \cdot \left. \frac{d\phi}{dE} \right|_{\text{source}}, \quad (19)$$

where $P_{\text{abs.}}$ represents the absorption probability by background photon and dark photon scattering.

IV. FITS TO GAMMA RAYS

To constrain oscillation effects we consider a combination of the recent 100+ TeV gamma ray data from

Tibet AS γ [2] and HAWC [6], together with previous measurements from HEGRA [3] and MAGIC [4]. The observed gamma ray spectrum is consistent with an expected Inverse-Compton (IC) emission spectrum from accelerated electrons inside the magnetized nebula. The shape of such an IC-dominated spectrum is proposed to follow a ‘parabola’ parametrization [69]

$$\frac{d\phi^{\text{IC}}}{dE} = \phi_0 \left(\frac{E}{E_0} \right)^{\alpha + \beta \log_{10}(E/E_0)}, \quad (20)$$

where the best-fit to AS γ , HEGRA, MAGIC and HAWC data gives $\alpha = -2.57$, $\beta = -0.17$. This best-fit parameters are obtained by minimizing the χ^2 function of joint fit

$$\chi^2 = \sum_j \sum_i \frac{(\Phi_i^{\text{th}} - f_j^{n-1} \cdot \Phi_{j,i})^2}{(f_j^{n-1} \cdot \delta\Phi_{j,i})^2} + \sum_j \frac{(f_j - 1)^2}{(\delta f_j)^2}, \quad (21)$$

where the subscript j denotes different experimental datasets and i is the i th spectral bin in each set. Φ^{th} is the integrated flux $E^n d\phi/dE$ in each bin (see Appendix A for details), where the raised energy-power index n matches experimental data formats. f_j is an energy scale uncertainty that accounts for the significant uncertainty in photon energy reconstruction in air shower measurements, which causes the flux spectrum to effectively shift in energy (and magnitude if $n \neq 1$). Such rescaling is typically in the 10% – 20% range and it is often necessary for the consistency between experiments. The fit with the IC spectrum gives the best scaling factors, as shown in Fig. 2. In our analysis we adopt $\delta f = 0.15$ for HEGRA [3], 0.15 for MAGIC, 0.12 for Tibet AS γ and 0.14 for HAWC. We restrict the variation of f_j to be within the range of energy scaling uncertainty $|\Delta f_j| \leq \delta f_j$.

The fits with axion and dark photon effects are performed after incorporating the photon flux suppression given in Eqs. (13) and (19). For ALP-induced oscillation, a best fit point is obtained at $g_{a\gamma\gamma} = 1.58 \times 10^{-11} \text{ GeV}^{-1}$, $m_a = 1.26 \times 10^{-7} \text{ eV}$ with the minimal $\chi_{\text{min}}^2 = 35.6$, giving a slight improvement over the background-only fit due to fluctuations in the measured energy spectra.

The fitting process marginalizes over the background IC spectral parameters $\{\phi_0, E_0, \alpha, \beta\}$ and experimental energy scaling factors $\{f_j\}$ to obtain the minimal χ^2 for each point in the ALP ($m_a, g_{a\gamma\gamma}$) and dark photon (m_D, ϵ) parameter spaces. The statistical significance of the χ^2 variation with ALP parameters needs special treatment due to the highly oscillatory dependence of the spectral deviation on these parameters. Following the statistical prescription for nonlinear dependence in Ref. [44], we compare likelihood distribution and find the oscillatory dependence on $g_{a\gamma\gamma}$ and m_a is equivalent to 3.5 effective degrees of freedom, which corresponds to a 95% C.L. increment $\Delta\chi^2 \sim 8.7$.

Interestingly, due to very low global χ_{min}^2 value, even with a $\Delta\chi^2 = 8.7$ increment, a $\chi^2 = 44.3$ is only slightly

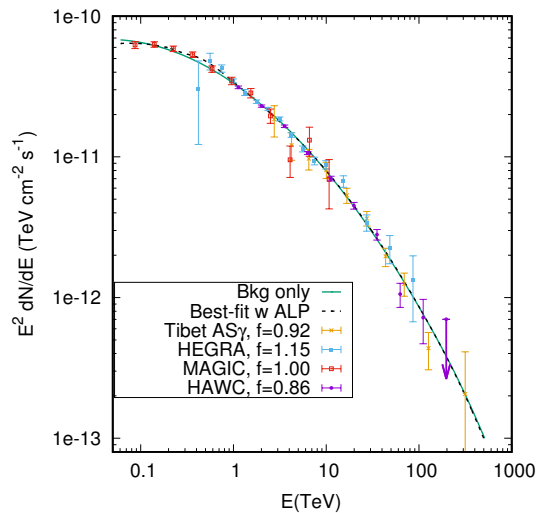


FIG. 2. Background-only fit (solid) and the best-fit with ALP effects (dashed) to Tibet AS γ [2], HAWC [6], HEGRA [3] and MAGIC [4] data. The energy scale factor f is allowed to float for each data set and its best-fit value is listed. Both the IC background (Eq. (20)) and ALP-case achieve good fits with $\chi^2 = 42.2/42$ and $\chi^2 = 35.6/38$, respectively. The ALP best-fit is found to be slightly better than background, although they agree to within 1σ .

worse (at 78% C.L.) than 1σ consistency for a χ^2 distribution with 38 effective degrees of freedom, and this is still a very acceptable global fit. Therefore, we use a more conservative criterion that requires the total χ^2 to

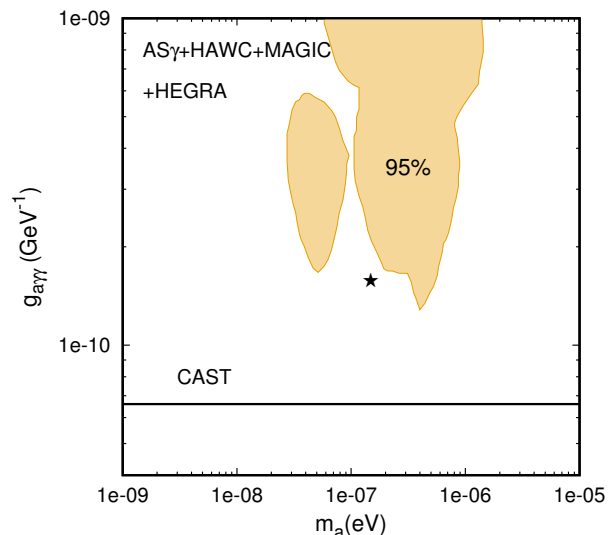


FIG. 3. ALP coupling and mass limits from fitting to Tibet AS γ , HAWC, HEGRA and MAGIC data. The filled contours show 95% C.L. exclusion regions with the total $\chi^2 = 53.4$. The best fit point $\chi_{\text{min}}^2 = 35.6$ is marked by an asterisk. The CAST limit [70] is shown for comparison.

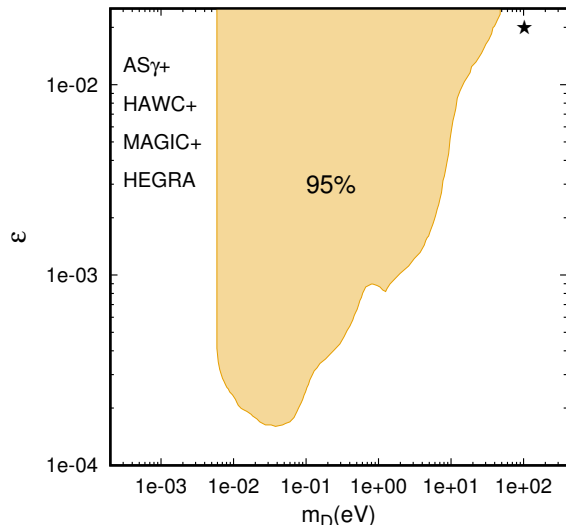


FIG. 4. The 95% C.L. exclusion region for gamma-ray scattering on dark photon as dark matter, from fitting to Tibet AS γ , HAWC, HEGRA and MAGIC data. The best fit $\chi^2_{\min}=38.0$ is marked by the asterisk point.

be below 53.4 for 95% consistency with all the data. The resulting exclusion contours on the $(m_a, g_{a\gamma\gamma})$ plane are shown in Fig. 3. For 95% exclusion around an ALP mass $2 \times 10^{-7} - 6 \times 10^{-7}$ eV, the gamma ray data give a limit of $g_{a\gamma\gamma}$ below 1.8×10^{-10} GeV $^{-1}$, which is close to the latest solar axion constraint from CAST [70].

As the spectral attenuation due to dark photon scattering is non-oscillatory, the 95% C.L. limit in Fig. 4 corresponds to a total $\chi^2 = 55.8$. The best exclusion of $\epsilon > 10^{-3}$ occurs at 10^{-2} eV $< m_D < 1$ eV. These dark photon ϵ limits are much higher than the typically small mixing required for A_D to decouple as dark matter, and significantly less stringent than other dark photon constraints [71].

Note the HESS experiment also observes high energy gamma rays from the Crab Nebula [5], and the resulting spectrum is well fit by the IC background. However, the very low χ^2 from HESS data is an overfit to the IC background model, and inclusion of this data set in the combined fit would lead to a less stringent constraint on new physics. Therefore, we do not include HESS in Fig. 3. For comparisons, we list the ALP fitting result to indi-

vidual data set, and the result after including HESS data, in Appendix B.

V. CONCLUSION

We have studied potential gamma ray spectral distortions induced by ALPs and dark photons in light of the recent measurement of photons above 100 TeV from the Tibet AS γ and HAWC experiments. The newly measured higher energy gamma ray events from the Crab Nebula allow us to extend beyond the sensitivity of previous studies to a higher ALP mass range. Assuming an astrophysical background spectrum from accelerated electron inverse Compton occurring scattering inside the Crab Nebula, we performed analyses on the data consistency with the IC background, including ALP-photon oscillation and attenuation effects due to photon-dark photon scattering.

The Tibet AS γ , HAWC data and previous HESS, MAGIC and HEGRA data are in very good consistency with a single parabola IC background, at the cost of shifting the energy scale of each experiment in a range comparable to their reported energy uncertainties. All of Tibet AS γ 's highest energy gamma ray events are from the Crab Nebula. The relatively close distance to the Earth makes the oscillation effects less significant compared to signals from farther away sources, but the higher energy photons involved can probe into the higher ALP mass range of $10^{-7} - 10^{-6}$ eV. For a mass region centred at $2 \times 10^{-7} - 6 \times 10^{-7}$ eV, the ALP-photon effective coupling is excluded to 1.8×10^{-10} GeV $^{-1}$. These limits may improve with future accumulation of extremely high energy gamma ray data, or 100+ TeV measurements from other identifiable sources at significant distances.

We also studied the flux attenuation from scattering on massive dark photons constituting all the dark matter in our Universe, which leads to $\epsilon \lesssim 10^{-3}$ for 10^{-2} eV $< m_D < 1$ eV. This is subdominant to the existing laboratory and cosmological bounds.

Acknowledgments

Y.G. thanks the Institute of High Energy Physics, CAS, for support by the grant no. Y95461A0U2 and partially by no. Y7515560U1. T.Li is supported by the National Natural Science Foundation of China under grant no. 11875062 and 11947302, and by the Key Research Program of Frontier Science, CAS. X.J.Bi is supported by NSFC under grant nos.U1738209 and 11851303.

-
- [1] Alberto Franceschini and Giulia Rodighiero, “The extragalactic background light revisited and the cosmic photon-photon opacity,” *Astron. Astrophys.* **603**, A34 (2017), arXiv:1705.10256 [astro-ph.HE].
- [2] M. Amenomori et al., “First Detection of Photons with Energy Beyond 100 TeV from an Astrophysical Source,”

Phys. Rev. Lett. **123**, 051101 (2019), arXiv:1906.05521 [astro-ph.HE].

- [3] F. Aharonian et al. (HEGRA), “The Crab nebula and pulsar between 500-GeV and 80-TeV. Observations with the HEGRA stereoscopic air Cerenkov telescopes,” *Astrophys. J.* **614**, 897–913 (2004), arXiv:astro-ph/0407118

- [astro-ph].
- [4] J. Aleksić et al. (MAGIC), “The major upgrade of the MAGIC telescopes, Part II: A performance study using observations of the Crab Nebula,” *Astropart. Phys.* **72**, 76–94 (2016), arXiv:1409.5594 [astro-ph.IM].
- [5] A. Abramowski et al. (H.E.S.S.), “H.E.S.S. Observations of the Crab during its March 2013 GeV Gamma-Ray Flare,” *Astron. Astrophys.* **562**, L4 (2014), arXiv:1311.3187 [astro-ph.HE].
- [6] A. U. Abeysekara et al. (HAWC), “Measurement of the Crab Nebula at the Highest Energies with HAWC,” (2019), arXiv:1905.12518 [astro-ph.HE].
- [7] Georg Raffelt and Leo Stodolsky, “Mixing of the Photon with Low Mass Particles,” *Phys. Rev.* **D37**, 1237 (1988).
- [8] Keith R. Dienes, Christopher F. Kolda, and John March-Russell, “Kinetic mixing and the supersymmetric gauge hierarchy,” *Nucl. Phys.* **B492**, 104–118 (1997), arXiv:hep-ph/9610479 [hep-ph].
- [9] Steven A. Abel, Joerg Jaeckel, Valentin V. Khoze, and Andreas Ringwald, “Illuminating the Hidden Sector of String Theory by Shining Light through a Magnetic Field,” *Phys. Lett.* **B666**, 66–70 (2008), arXiv:hep-ph/0608248 [hep-ph].
- [10] Sidney R. Coleman and Sheldon L. Glashow, “Cosmic ray and neutrino tests of special relativity,” *Phys. Lett.* **B405**, 249–252 (1997), arXiv:hep-ph/9703240 [hep-ph].
- [11] G. Amelino-Camelia, John R. Ellis, N. E. Mavroumatos, Dimitri V. Nanopoulos, and Subir Sarkar, “Tests of quantum gravity from observations of gamma-ray bursts,” *Nature* **393**, 763–765 (1998), arXiv:astro-ph/9712103 [astro-ph].
- [12] Petr Satunin, “New constraints on Lorentz Invariance violation from Crab Nebula spectrum beyond 100 TeV,” (2019), arXiv:1906.08221 [astro-ph.HE].
- [13] John Preskill, Mark B. Wise, and Frank Wilczek, “Cosmology of the Invisible Axion,” *Phys. Lett.* **120B**, 127–132 (1983).
- [14] L. F. Abbott and P. Sikivie, “A Cosmological Bound on the Invisible Axion,” *Phys. Lett.* **120B**, 133–136 (1983).
- [15] Michael Dine and Willy Fischler, “The Not So Harmless Axion,” *Phys. Lett.* **120B**, 137–141 (1983).
- [16] Wayne Hu, Rennan Barkana, and Andrei Gruzinov, “Cold and fuzzy dark matter,” *Phys. Rev. Lett.* **85**, 1158–1161 (2000), arXiv:astro-ph/0003365 [astro-ph].
- [17] Lam Hui, Jeremiah P. Ostriker, Scott Tremaine, and Edward Witten, “Ultralight scalars as cosmological dark matter,” *Phys. Rev.* **D95**, 043541 (2017), arXiv:1610.08297 [astro-ph.CO].
- [18] Joerg Jaeckel and Andreas Ringwald, “The Low-Energy Frontier of Particle Physics,” *Ann. Rev. Nucl. Part. Sci.* **60**, 405–437 (2010), arXiv:1002.0329 [hep-ph].
- [19] Igor G. Irastorza and Javier Redondo, “New experimental approaches in the search for axion-like particles,” *Prog. Part. Nucl. Phys.* **102**, 89–159 (2018), arXiv:1801.08127 [hep-ph].
- [20] Eduard Masso, “Axions and their relatives,” *Lect. Notes Phys.* **741**, 83–94 (2008), arXiv:hep-ph/0607215.
- [21] Csaba Csaki, Nemanja Kaloper, Marco Peloso, and John Terning, “Super GZK photons from photon axion mixing,” *JCAP* **0305**, 005 (2003), arXiv:hep-ph/0302030 [hep-ph].
- [22] Alessandro De Angelis, Marco Roncadelli, and Oriana Mansutti, “Evidence for a new light spin-zero boson from cosmological gamma-ray propagation?” *Phys. Rev.* **D76**, 121301 (2007), arXiv:0707.4312 [astro-ph].
- [23] Alessandro De Angelis, Giorgio Galanti, and Marco Roncadelli, “Relevance of axion-like particles for very-high-energy astrophysics,” *Phys. Rev.* **D84**, 105030 (2011), [Erratum: *Phys. Rev.* D87,no.10,109903(2013)], arXiv:1106.1132 [astro-ph.HE].
- [24] Melanie Simet, Dan Hooper, and Pasquale D. Serpico, “The Milky Way as a Kiloparsec-Scale Axionscope,” *Phys. Rev.* **D77**, 063001 (2008), arXiv:0712.2825 [astro-ph].
- [25] Malcolm Fairbairn, Timur Rashba, and Sergey V. Troitsky, “Photon-axion mixing and ultra-high-energy cosmic rays from BL Lac type objects - Shining light through the Universe,” *Phys. Rev.* **D84**, 125019 (2011), arXiv:0901.4085 [astro-ph.HE].
- [26] Manuel Meyer, Dieter Horns, and Martin Raue, “First lower limits on the photon-axion-like particle coupling from very high energy gamma-ray observations,” *Phys. Rev.* **D87**, 035027 (2013), arXiv:1302.1208 [astro-ph.HE].
- [27] A. Dominguez, M. A. Sanchez-Conde, and F. Prada, “Axion-like particle imprint in cosmological very-high-energy sources,” *JCAP* **1111**, 020 (2011), arXiv:1106.1860 [astro-ph.CO].
- [28] Alessandro Mirizzi and Daniele Montanino, “Stochastic conversions of TeV photons into axion-like particles in extragalactic magnetic fields,” *JCAP* **0912**, 004 (2009), arXiv:0911.0015 [astro-ph.HE].
- [29] Alessandro Mirizzi, Georg G. Raffelt, and Pasquale D. Serpico, “Signatures of Axion-Like Particles in the Spectra of TeV Gamma-Ray Sources,” *Phys. Rev.* **D76**, 023001 (2007), arXiv:0704.3044 [astro-ph].
- [30] A De Angelis, O Mansutti, M Persic, and M Roncadelli, “Photon propagation and the very high energy γ -ray spectra of blazars: how transparent is the universe?” *Monthly Notices of the Royal Astronomical Society: Letters* **394**, L21–L25 (2009).
- [31] M. A. Sanchez-Conde, D. Paneque, E. Bloom, F. Prada, and A. Dominguez, “Hints of the existence of Axion-Like-Particles from the gamma-ray spectra of cosmological sources,” *Phys. Rev.* **D79**, 123511 (2009), arXiv:0905.3270 [astro-ph.CO].
- [32] Alexander V. Belikov, Lisa Goodenough, and Dan Hooper, “No Indications of Axion-Like Particles From Fermi,” *Phys. Rev.* **D83**, 063005 (2011), arXiv:1007.4862 [astro-ph.HE].
- [33] A. Abramowski et al. (H.E.S.S.), “Constraints on axionlike particles with H.E.S.S. from the irregularity of the PKS 2155-304 energy spectrum,” *Phys. Rev.* **D88**, 102003 (2013), arXiv:1311.3148 [astro-ph.HE].
- [34] Rebecca Reesman and T. P. Walker, “Probing the Scale of ALP Interactions with Fermi Blazars,” *JCAP* **1408**, 021 (2014), arXiv:1402.2533 [astro-ph.HE].
- [35] Alexandre Payez, Carmelo Evoli, Tobias Fischer, Maurizio Giannotti, Alessandro Mirizzi, and Andreas Ringwald, “Revisiting the SN1987A gamma-ray limit on ultralight axion-like particles,” *JCAP* **1502**, 006 (2015), arXiv:1410.3747 [astro-ph.HE].
- [36] Bijan Berenji, Jennifer Gaskins, and Manuel Meyer, “Constraints on Axions and Axionlike Particles from Fermi Large Area Telescope Observations of Neutron Stars,” *Phys. Rev.* **D93**, 045019 (2016), arXiv:1602.00091 [astro-ph.HE].
- [37] M. Ajello et al. (Fermi-LAT), “Search for Spectral Irreg-

- ularities due to Photon–Axionlike-Particle Oscillations with the Fermi Large Area Telescope,” *Phys. Rev. Lett.* **116**, 161101 (2016), arXiv:1603.06978 [astro-ph.HE].
- [38] M. Meyer, M. Giannotti, A. Mirizzi, J. Conrad, and M. A. Sánchez-Conde, “Fermi Large Area Telescope as a Galactic Supernovae Axionscope,” *Phys. Rev. Lett.* **118**, 011103 (2017), arXiv:1609.02350 [astro-ph.HE].
- [39] Jhilik Majumdar, Francesca Calore, and Dieter Horns, “Spectral modulation of non-galactic plane gamma-ray pulsars due to photon-alps mixing in galactic magnetic field,” arXiv preprint arXiv:1711.08723 (2017).
- [40] Giorgio Galanti and Marco Roncadelli, “Extragalactic photon–axion-like particle oscillations up to 1000 TeV,” *JHEAp* **20**, 1–17 (2018), arXiv:1805.12055 [astro-ph.HE].
- [41] Sergey Troitsky, “Towards discrimination between galactic and intergalactic axion-photon mixing,” *Phys. Rev.* **D93**, 045014 (2016), arXiv:1507.08640 [astro-ph.HE].
- [42] Kazunori Kohri and Hideo Kodama, “Axion-Like Particles and Recent Observations of the Cosmic Infrared Background Radiation,” *Phys. Rev.* **D96**, 051701 (2017), arXiv:1704.05189 [hep-ph].
- [43] Yun-Feng Liang, Cun Zhang, Zi-Qing Xia, Lei Feng, Qiang Yuan, and Yi-Zhong Fan, “Constraints on axion-like particle properties with TeV gamma-ray observations of Galactic sources,” *JCAP* **1906**, 042 (2019), arXiv:1804.07186 [hep-ph].
- [44] Cun Zhang, Yun-Feng Liang, Shang Li, Neng-Hui Liao, Lei Feng, Qiang Yuan, Yi-Zhong Fan, and Zhong-Zhou Ren, “New bounds on axionlike particles from the Fermi Large Area Telescope observation of PKS 2155-304,” *Phys. Rev.* **D97**, 063009 (2018), arXiv:1802.08420 [hep-ph].
- [45] Maxim Libanov and Sergey Troitsky, “On the impact of magnetic-field models in galaxy clusters on constraints on axion-like particles from the lack of irregularities in high-energy spectra of astrophysical sources,” (2019), arXiv:1908.03084 [astro-ph.HE].
- [46] G. B. Long, W. P. Lin, P. H. T. Tam, and W. S. Zhu, “Testing CIBER cosmic infrared background measurements and axionlike particles with observations of TeV blazars,” (2019), arXiv:1912.05309 [astro-ph.HE].
- [47] Zi-Qing Xia, Yun-Feng Liang, Lei Feng, Qiang Yuan, Yi-Zhong Fan, and Jian Wu, “Searching for the possible signal of the photon-axionlike particle oscillation in the combined GeV and TeV spectra of supernova remnants,” *Phys. Rev.* **D100**, 123004 (2019), arXiv:1911.08096 [astro-ph.HE].
- [48] G. I. Rubtsov and S. V. Troitsky, “Breaks in gamma-ray spectra of distant blazars and transparency of the Universe,” *JETP Lett.* **100**, 355–359 (2014), [*Pisma Zh. Eksp. Teor. Fiz.*100,no.6,397(2014)], arXiv:1406.0239 [astro-ph.HE].
- [49] Giorgio Galanti, Fabrizio Tavecchio, Marco Roncadelli, and Carmelo Evoli, “Blazar VHE spectral alterations induced by photon–ALP oscillations,” *Mon. Not. Roy. Astron. Soc.* **487**, 123–132 (2019), arXiv:1811.03548 [astro-ph.HE].
- [50] Hendrik Vogel, Ranjan Laha, and Manuel Meyer, “Diffuse axion-like particle searches,” arXiv preprint arXiv:1712.01839 (2017).
- [51] Giorgio Galanti and Marco Roncadelli, “Behavior of axionlike particles in smoothed out domainlike magnetic fields,” *Phys. Rev. D* **98**, 043018 (2018), arXiv:1804.09443 [astro-ph.HE].
- [52] Pierre Fayet, “Effects of the Spin 1 Partner of the Goldstino (Gravitino) on Neutral Current Phenomenology,” *Phys. Lett.* **95B**, 285–289 (1980).
- [53] Bob Holdom, “Two U(1)’s and Epsilon Charge Shifts,” *Phys. Lett.* **166B**, 196–198 (1986).
- [54] R. Ruffini, G. V. Vereshchagin, and S. S. Xue, “Cosmic absorption of ultra high energy particles,” *Astrophys. Space Sci.* **361**, 82 (2016), arXiv:1503.07749 [astro-ph.HE].
- [55] A. P. Lobanov, H. S. Zechlin, and D. Horns, “Astrophysical searches for a hidden-photon signal in the radio regime,” *Phys. Rev.* **D87**, 065004 (2013), arXiv:1211.6268 [astro-ph.CO].
- [56] Andrea Caputo, Hongwan Liu, Siddharth Mishra-Sharma, and Joshua T. Ruderman, “Dark Photon Oscillations in Our Inhomogeneous Universe,” (2020), arXiv:2002.05165 [astro-ph.CO].
- [57] Alessandro Mirizzi, Javier Redondo, and Gunter Sigl, “Microwave Background Constraints on Mixing of Photons with Hidden Photons,” *JCAP* **0903**, 026 (2009), arXiv:0901.0014 [hep-ph].
- [58] Hannes-Sebastian Zechlin, Dieter Horns, and Javier Redondo, “New constraints on hidden photons using very high energy gamma-rays from the crab nebula,” in *AIP Conference Proceedings*, Vol. 1085 (American Institute of Physics, 2008) pp. 727–730.
- [59] Jihn E. Kim, “Weak Interaction Singlet and Strong CP Invariance,” *Phys. Rev. Lett.* **43**, 103 (1979).
- [60] Mikhail A. Shifman, A. I. Vainshtein, and Valentin I. Zakharov, “Can Confinement Ensure Natural CP Invariance of Strong Interactions?” *Nucl. Phys.* **B166**, 493–506 (1980).
- [61] A. R. Zhitnitsky, “On Possible Suppression of the Axion Hadron Interactions. (In Russian),” *Sov. J. Nucl. Phys.* **31**, 260 (1980), [*Yad. Fiz.*31,497(1980)].
- [62] Michael Dine, Willy Fischler, and Mark Srednicki, “A Simple Solution to the Strong CP Problem with a Harmless Axion,” *Phys. Lett.* **104B**, 199–202 (1981).
- [63] Georg Raffelt and Leo Stodolsky, “Mixing of the photon with low-mass particles,” *Phys. Rev. D* **37**, 1237–1249 (1988).
- [64] Manuel Meyer, Daniele Montanino, and Jan Conrad, “On detecting oscillations of gamma rays into axionlike particles in turbulent and coherent magnetic fields,” *JCAP* **09**, 003 (2014), arXiv:1406.5972 [astro-ph.HE].
- [65] Alexandra Dobrynina, Alexander Kartavtsev, and Georg Raffelt, “Photon-photon dispersion of TeV gamma rays and its role for photon-ALP conversion,” *Phys. Rev. D* **91**, 083003 (2015), [Erratum: *Phys.Rev.D* 95, 109905 (2017)], arXiv:1412.4777 [astro-ph.HE].
- [66] Silvia Vernetto and Paolo Lipari, “Absorption of very high energy gamma rays in the Milky Way,” *Phys. Rev.* **D94**, 063009 (2016), arXiv:1608.01587 [astro-ph.HE].
- [67] Ronnie Jansson and Glennys R. Farrar, “The Galactic Magnetic Field,” *Astrophys. J.* **761**, L11 (2012), arXiv:1210.7820 [astro-ph.GA].
- [68] Jean-François Fortin and Kuver Sinha, “Photon-Dark Photon Conversions in Background Electromagnetic Fields,” (2019), arXiv:1904.08968 [hep-ph].
- [69] D. Zaborov, A. M. Taylor, D. A. Sanchez, J. P. Lenain, and C. Romoli (H.E.S.S.), “Gamma-ray blazar spectra with H.E.S.S. II mono analysis: The case of PKS 2155–304 and PG 1553+113,” *AIP Conf. Proc.* **1792**, 050017 (2017), arXiv:1612.05111 [astro-ph.HE].

- [70] V. Anastassopoulos et al. (CAST), “New CAST Limit on the Axion-Photon Interaction,” *Nature Phys.* **13**, 584–590 (2017), arXiv:1705.02290 [hep-ex].
- [71] Rouven Essig, John A Jaros, William Wester, P Hansson Adrian, S Andreas, T Averett, O Baker, B Batell, M Battaglieri, J Beacham, et al., “Dark sectors and new, light, weakly-coupled particles,” arXiv preprint arXiv:1311.0029 (2013).

Appendix A: Flux binning & scaling

The energy uncertainty of terrestrial cosmic ray experiments is generally non-negligible thus the smearing of the observed energy needs to be incorporated. The energy resolution of AS γ ranges from 20% to 40% [2] and we adopt 30% for this analysis. Similarly, the energy resolution for HEGRA, MAGIC and HAWC is taken as $\delta = 10\%$ [3], 16% [4] and 23% [6] of the detected energy. The observed spectrum is then convoluted with a normally distributed energy around the ‘true’ energy from the incoming spectrum.

For a detector measuring a photon in one energy bin ranging from E_0 to $E_0 + \Delta E$, the expected flux is

$$\Delta\phi = \int_{E_0}^{E_0+\Delta E} dE \int_0^\infty A(E', E) \frac{d\phi}{dE'} dE' \quad (\text{A1})$$

where E and E' are the observed and ‘true’ cosmic energies, A is a window function that takes account of E' being observed at E with a normally distributed probability with energy uncertainty $\delta \cdot E$, and $\frac{d\phi}{dE'}$ is the incoming differential energy flux. After integrating over the energy bin the expected flux is,

$$\Delta\phi = \int_0^\infty \tilde{A}(E', E_0, \Delta E) \frac{d\phi}{dE'} dE', \quad (\text{A2})$$

where the integrated $\tilde{A}(E', E_0, E_0 + \Delta E)$ takes the form

$$\tilde{A} = \frac{1}{2} \left[\text{erf} \left(\frac{E_0 + \Delta E - E'}{\sqrt{2}\delta \cdot E'} \right) - \text{erf} \left(\frac{E_0 - E'}{\sqrt{2}\delta \cdot E'} \right) \right], \quad (\text{A3})$$

where ‘erf’ is the usual Gaussian error function. After spectral smearing, we still need to consider an overall spectral shift due to the experimental energy scaling uncertainty, $E \rightarrow f \cdot E$. The flux in an f -shifted energy bin is

$$\Delta\phi = \int_0^\infty \tilde{A}(E', f \cdot E_0, f \cdot \Delta E) f^n \cdot \frac{d\phi}{dE'} dE'. \quad (\text{A4})$$

Often the experimental data are given in the form of binned flux multiplied by E^n . Without assumptions on the incoming spectrum, shifted experimental data are treated as $E^n \frac{d\phi}{dE} \rightarrow f^{n-1} \cdot E^n \frac{d\phi}{dE}$, maintaining the same event counts in the (shifted) energy bin.

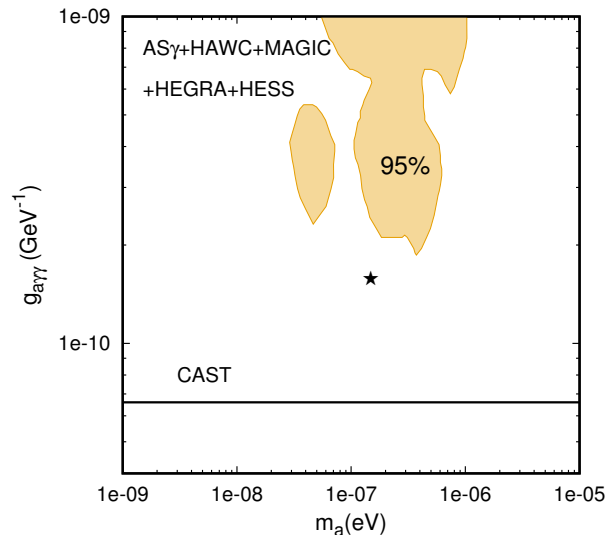


FIG. 5. Similar to Fig. 3, ALP oscillation limits with all five data sets. The best fit $\chi_{\min}^2=57.8$ is marked by the asterisk point.

Appendix B: Comparisons with HESS data

Here we list the IC background fitting result to individual experiments, and also the ALP-oscillated fitting results after including HESS data into the joint analysis.

TABLE I. Inverse-Compton spectrum fits to each experiment. ϕ_0 and E_0 take unit of $\text{TeV cm}^2\text{s}^{-1}$ and TeV .

Data	χ_{\min}^2	d.o.f.	ϕ_0	E_0	α	β
Tibet AS γ [2]	1.8	6	9.28×10^{-12}	1.47	-2.12	-0.32
HEGRA [3]	13.6	12	1.58×10^{-12}	3.02	-2.65	-0.11
MAGIC [4]	6.6	7	9.96×10^{-13}	3.79	-2.80	-0.25
HESS [5]	14.8	28	2.04×10^{-13}	6.44	-2.79	-4.06×10^{-3}
HAWC [6]	6.5	5	1.68×10^{-11}	1.44	-2.49	-0.16

Table. I shows the dataset background consistency with the best fitting results to Inverse Compton spectrum in Eq. (20) after considering the absorption effect due to the background photons. The reduced χ^2 values from AS γ and HESS fits are significantly less than one, indicating their combination with other data sets may loosen constraints on spectral distortions. As the new AS γ data above 100 TeV are necessary for testing axions at higher mass ranges, we only include AS γ in Section IV. The five-set joint result with HESS included is shown in Fig. 5, where the 95% exclusion region moves slightly to larger $g_{a\gamma\gamma}$.